Desalination and Water Treatment
www.deswater.com

doi: 10.5004/dwt.2018.21958

108 (2018) 152–163
March

Adsorptive removal of boron from aqueous solutions with selective resins in high-depth fixed-bed columns

Yu Chang Kim*, Sungyun Lee

Department of Environmental Machinery, Korea Institute of Machinery and Materials, Daejeon 34103, Korea, Tel. +82-42-868-7397; email: kimyc@kimm.re.kr (Y.C. Kim)

Received 29 September 2017; Accepted 25 January 2018

ABSTRACT

Adsorption method using boron-specific resins is known to be effective for the selective removal from desalinated seawater. This article analyses the performance of high-depth fixed-bed columns for the removal of boron from aqueous solutions. First, the effects of three kinds of resins, flow rates (3, 5, 7, and 10 L/h), bed depths (80, 120, and 160 cm), flow directions (upward and downward), and influent boron concentrations (2.5 and 5 mg/L) on breakthrough curves were investigated. The breakthrough curves obtained in high-depth fixed-bed columns were dependent on the parameters tested. Second, the experimental data were validated by some empirical column adsorption models, such as the Thomas, Yoon–Nelson, Adams–Bohart, and bed-depth service-time models. The breakthrough curves obtained from high-depth column experiments were in good agreement with model predictions. The contact time between adsorbent and adsorbate is an important factor for adsorptive removal. Flow rate and bed depth, affecting the pressure drop, were two critical control parameters for adjusting the contact time. Finally, sensitivity analysis revealed how boron influent concentration, bed mass, flow discharge, rate constant, and adsorption capacity influenced the shape of the breakthrough curve.

Keywords: Boron removal; Boron selective resin; Adsorption; Fixed-bed column; Breakthrough curve; Desalination

1. Introduction

The global average boron concentration is reportedly 13 ppb in fresh river water and 5 ppm (mg/L) in seawater [1,2]. Although boron is a very necessary nutrient for plant growth, it can have a harmful or damaging effect when its concentration exceeds certain limits in irrigation water [3,4]. Accordingly, boron is of special concern in irrigation water. However, the influence of boron on human health is still the subject of discussion and some countries have not yet established drinking water levels [3–7]. In 2011, the Drinking-Water Quality Committee of the World Health Organization (WHO) revised the boron guideline value to 2.4 mg/L [4,6–8]. This requirement has affected the design of seawater reverse osmosis desalination plants. Nevertheless, many utilities still set product water limits from seawater desalination plants as low as 0.5 mg/L, reflecting agricultural issues [1,3].

The membranes available presently for seawater desalination remove only 60%–80% of boron in a single reverse osmosis (RO) pass [3,9], so the permeate of a single pass contains 1–2 mg/L of boron [3,4,9,10]. Thus, seawater should be desalinated in a two-pass RO process [3,4,9,10]. A proportion of the permeate (rear side) of the first pass is treated again in a second pass. However, the second-pass RO consumes additional energy [3,4,9]. Furthermore, among several conventional treatment processes, such as precipitation–coagulation, RO, electrodialysis, solvent extraction, membrane filtration, and adsorption with selective ion exchange resins for boron removal, the adsorption method is widely considered to be the most promising and robust process to purify aqueous solutions due to its ease of implementation, low cost, and high efficiency [4,6,8,9].

In recent years, boron-selective resins (BSRs), based on chelation, have attracted much interest due to their selectivity

* Corresponding author.

and high capacity [4–6,8,9,11–15]. The use of BSRs based on macroporous polystyrene matrices with active *N*-methyl-d-glucamine (NMDG) groups seems to be the most promising way to remove boron from aqueous solutions [4,8,13–16]. The presence of two vicinal hydroxyls in the NMDG group allows boric acid and borates to form stable complexes with the resin via a covalent bond [2,4,8,12,14,15,17,18]. The adsorption process with BSRs is advantageous over second-pass RO (i.e., BWRO) because it is not greatly affected by operating conditions, such as salinity, temperature, or pH [4]. In particular, the adsorptive resin bed requires much less pumping energy than BWRO [9,10]. Additionally, water recovery from the BSR bed column is nearly 100%, whereas that of second-pass RO is 80%–90% [10]. Thus, if low total dissolved solids (TDS) is not a requirement, adsorption with BSRs can be used for boron removal from the permeate from first-pass RO.

To our knowledge, most previous studies on boron elimination by BSRs have been performed in glass jars and small-scale columns [5,6,12,13,15,17,19,20]. Breakthrough data using large-scale columns are rare because of the long breakthrough times and high analytical costs. Bench-scale experiments are better suited for the study of BSRs, rather than for the study of the adsorption process and its optimisation. Generally, batch experiments in glass jars are used to determine equilibrium isotherms and the kinetics of boron removal on to resin particles. Also, predictions based on a rapid, small-scale column test would overestimate adsorption capacity. The results obtained from small-scale columns are radically different from those of a large-scale column due to different flow stream conditions as well [2,14]. Additionally, bench-scale experiments do not provide reasonable information about several hydrodynamic parameters of fixed-bed columns. Thus, a careful approach must be taken regarding adsorption processes when applying test data obtained from laboratory-scale experiments to large-scale processes. Because the breakthrough curve obtained in high-depth columns carries information about the dynamic behaviour of the fixed-bed columns, large-scale tests are strongly recommended when designing full-scale adsorption processes.

The objectives of the present study were to: (a) augment the database of boron breakthrough curves based on high-depth fixed-bed columns; (b) investigate the effects of three kinds of resins, flow rates, bed depths, flow directions, and influent boron concentrations on boron breakthrough curves; (c) validate the experimental data obtained in high-depth columns using empirical models, such as the Thomas, Yoon–Nelson, Adams–Bohart, and bed-depth service-time (BDST) models; (d) analyse the effects of flow rates and bed depths on the pressure drop and the corresponding specific energy consumption in the high-depth columns; and (e) perform sensitivity analyses to confirm the effects of model parameters on breakthrough curve shapes.

2. Experimental

2.1. Adsorbent and adsorbate

Commercially available BSRs as adsorbents are based on copolymers of styrene and divinylbenzene [4,8,13,14,16]. Although these resins come from different companies, they are crosslinked macroporous polystyrene resins, with the active group NMDG. For this study, three commercial resins from different manufacturers were selected: PWA10 (Dow, USA), S108 (Purolite, USA), and MK51 (Lanxess, Germany). Because these BSRs should be fully hydrated prior to packing into the column, the resin beads were immersed in deionised water for 24 h before being packed into the column [21]. Table 1 lists the specifications of these resins [22–25]. According to the specifications provided by the manufacturer, the total exchange capacities of the PWA10, S108, and MK51 resins in equivalents were 0.7, 0.6, and 0.8 eq/L, respectively.

For adsorbate, boric acid solutions were prepared by dissolving the appropriate amount of boric acid in tap water because boron exists in the form of boric acid in environmental water [3,4,8]. Two synthetic solutions containing 2.5 and 5 mg/L of boron in tap water were used as feed solutions.

2.2. Column mode experiments

Fig. 1 presents a schematic diagram of the column setup used for the fixed-bed studies. Because columns with a diameter greater than 2 cm can usually be scaled up linearly [21], the experimental setup was composed of nine columns with inner diameters of 2 cm and heights of 160 cm. For upflow operation, six columns, whose height was the same as the bed depth, were also used. Depending on the objective of the experiments, three, six, and nine columns were operated simultaneously for each experiment. Rotameters and differential pressure gauges were installed for the flow and differential pressure measurement in each column, respectively.

The adsorption experiments using fixed-bed columns were performed with different resins, flow rates, bed depths, influent boron concentrations, and flow directions. The column experiments were continued until complete saturation of the resins was achieved. Adsorption is a time-dependent process and the optimal specific flow rates are from 10 to 40 BV/h [21,22,24]. Here, BV means the dimensionless bed volume (i.e., volume of fluid per volume of resin). Accordingly, we used feed flow rates to the column between 11.95 and 39.84 BV/h. For experiments using nine columns with 80 cm bed depths, three flow rates (3, 5, and 7 L/h) were applied,

Table 1
Physical and chemical properties of three kinds of boron specific resins used in this study

	Product name	Company	Effective diameter (μm)	Median diameter (μm)	Bulk density (g/L)	Total capacity (eq/L)
1	PWA10	Dow (Rohm and Haas)	550–600	575	700	0.7
2	S108	Purolite	425–630	527.5	700	0.6
3	MK51	Lanxess	440–540	490	710	0.8

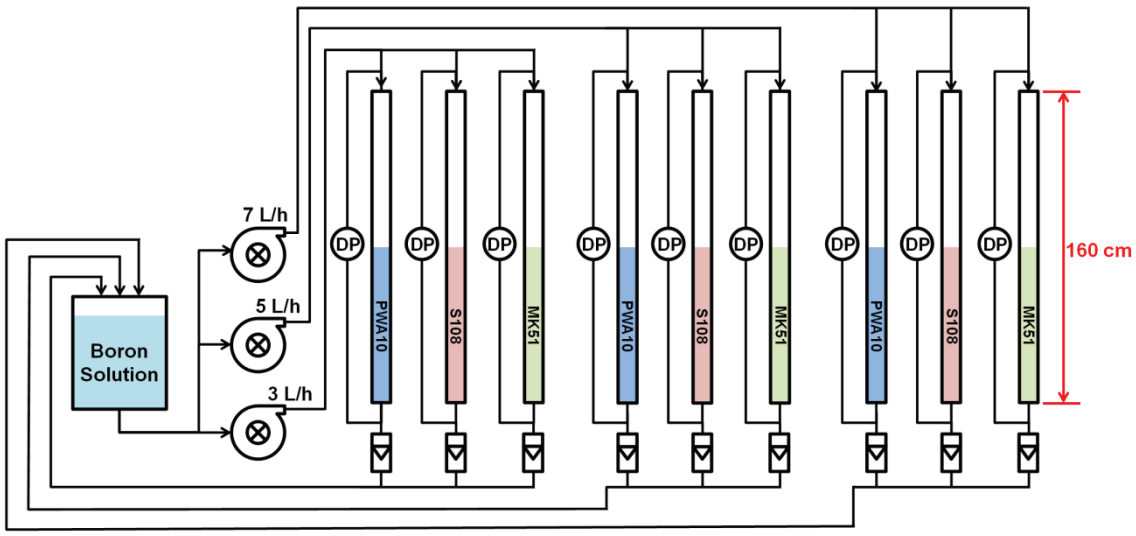

Fig. 1. Schematic diagram of a high-depth adsorptive column setup for boron removal. Rotameters and differential pressure gauges (D_p) were installed for the flow and differential pressure measurement in each column, respectively. This setup is one example of the configuration just for investigating the effect of flow rates and different resins on breakthrough curves.

while for experiments using six and three columns with three bed depths, flow rates of 10 and 7 L/h were used, respectively. To change bed depth, these columns were filled with resin up to 80, 120, and 160 cm, corresponding to bed volumes of 251, 377, and 502 cm^3, respectively. To assess the effect of flow direction, the boron solution was passed through the resin bed in upflow or downflow mode. All experiments were conducted at room temperature.

The effluent solution sample was collected from the outlet of the column at regular time intervals of 1 h, but the boron concentration of the effluent was analysed only at the selected time interval of 7 or 8 h. This time interval was sufficient to obtain a breakthrough curve that ultimately determined the operation and dynamic response of the adsorption column. When the boron concentration in the effluent (C_t) became equal to the initial concentration in the influent (C_0), the flow was stopped. The threshold value, called the breakpoint concentration, was set as an effluent boron concentration of 0.5 mg/L.

2.3. Analysis of boron

Boron in aqueous samples can be analysed by spectrophotometric methods, based on colourimetric reactions of boron with specific reagents, such as curcumine, carmine, and azomethine-H [3,15,16]. In the present study, the boron concentration was measured with a Hach DR-6000 spectrophotometer by an azomethine-H method, which is known to be a convenient and a relatively accurate method. The measurement wavelength was 414 nm.

2.4. Kinetic models

In the design of a fixed-bed column adsorption process, the concentration-time profiles for the effluent are most important [21,26-28]. Thus, some empirical breakthrough curve models are used to describe the dynamic behaviour of the fixed-bed column. Here, three empirical models, based on non-linear regression analysis, the Thomas (T) [5,26,28,29], Yoon–Nelson (YN) [5,26,28,29], and Adams–Bohart (AB) [26,29] models, were applied to the experimental data to predict the breakthrough curves while a BDST model [26,28], based on linear regression, was used to predict the time needed for breakthrough under other conditions. Table 2 shows the non-linear mathematical expression, linearised form, linear dependence, and model parameters for each model. Model parameters can be determined from the linear dependence.

The characteristics of each model are as follows. The Thomas (T) model is one of the most widely used kinetic models to study column performance, assuming the adsorption obeys second-order reversible reaction kinetics and it is not limited by the chemical reaction but controlled by the mass transfer at the interface [5,26,28,29]. The Yoon–Nelson (YN) model is a relative simple model because it requires no detailed data concerning the characteristics of adsorbate, the type of adsorbent, or the physical properties of the adsorption bed [5,26,28,29]. This Yoon–Nelson model is based on the assumption that the rate of decrease in the probability of adsorption for each adsorbate molecule is directly proportional to the probability of the adsorbate molecule adsorption and the adsorbate breakthrough on the adsorbent. The initial region of the breakthrough curve can be well described by the Adams–Bohart (AB) model which assumes that the adsorption rate is related to both the residual capacity of the adsorbent and the concentration of the adsorbate, determined mainly by surface reactions on the adsorbent surface sites [26,29]. The BDST model is used to predict the time needed for breakthrough under other conditions without further experimental runs [26,28]. In this model, the adsorption rate is assumed to be regulated by the surface reaction between the adsorbate and the unused adsorbent.

Table 2
Linearised forms of used models and the corresponding model parameters

Model	Non-linear empirical equation and its linearised form	Linear dependence	Model parameter
Thomas	$\frac{C_t}{C_0}=\frac{1}{1+\exp\left(k_T q_e m Q^{-1}-k_T C_0 t\right)}$	$\ln\left(\frac{C_0-C_t}{C_t}\right)$ vs. t	k_T, q_e
	$\ln\left(\frac{C_0-C_t}{C_t}\right)=\frac{k_T\cdot q_e\cdot m}{Q}-k_T\cdot C_0\cdot t$		
Yoon–Nelson	$\frac{C_t}{C_0}=\frac{\exp\left(k_{YN}t-\tau k_{YN}\right)}{1+\exp\left(k_{YN}t-\tau k_{YN}\right)}$	$\ln\left(\frac{C_t}{C_0-C_t}\right)$ vs. t	k_{YN}, τ
	$\ln\left(\frac{C_t}{C_0-C_t}\right)=k_{YN}\cdot t-k_{YN}\cdot\tau$		
Adams–Bohart	$\frac{C_t}{C_0}=\exp\left(k_{AB}C_0 t-k_{AB}N_0 H V^{-1}\right)$	$\ln\left(\frac{C_t}{C_0}\right)$ vs. t	k_{AB}, N_0
	$\ln\left(\frac{C_t}{C_0}\right)=k_{AB}\cdot C_0\cdot t-k_{AB}\cdot N_0\cdot\frac{H}{\nu}$		
BDST	$t=\frac{N_0}{C_0\nu}H-\frac{1}{k_{BDST}C_0}\ln\left(\frac{C_0}{C_t}-1\right)$	t vs. H	k_{BDST}, N_0

Note: C_0, influent adsorbate concentration (mg/L); C_t, effluent adsorbate concentration (mg/L) at time t; k_T, Thomas rate constant (L/mg h); q_e, equilibrium boron uptake per gram of the adsorbent (mg/g); m, amount of adsorbent in the column (g); Q, volumetric flow rate (L/h); t, service time (h); k_{YN}, Yoon–Nelson rate constant (h^{-1}); τ, time required for 50% adsorbate breakthrough (h); k_{AB}, Adams–Bohart rate constant (L/mg h); N_0, adsorption capacity of the bed (mg/L); H, bed depth (m); ν, linear flow velocity (m/h); and k_{BDST}, BDST rate constant (L/mg h).

3. Results and discussion

3.1. Effects of different resins on breakthrough curves

Various BSRs are available commercially and their specifications can be obtained. Usually, the performance of a BSR depends on its polymeric support and functional groups. But even if BSRs have the same NMDG functional groups, they can exhibit different adsorption performances because of differing macroporous matrix structures [8]. Normally, their adsorption performances are not obtained in large-column mode but in small-batch mode experiments. Thus, a screening test for the selection of BSR adsorbents was performed using nine continuous flow fixed-bed columns under identical operating conditions. The bed depths of all columns were 80 cm (i.e., freeboard of 80 cm) and the influent boron concentration was 2.5 mg/L. Figs. 2(a)–(c) compare the performances of the three kinds of BSRs obtained for different flow rates of 3, 5, and 7 L/h, respectively. The dynamic behaviours of the nine fixed-bed columns were described in terms of the effluent concentration-time profile (i.e., the breakthrough curve). The value of C_t/C_0 in breakthrough curves is the dimensionless normalised effluent concentration. After some time, adsorbate breakthrough occurred and the effluent concentration increased with time. For each flow rate, PWA10 resin had the smallest breakthrough capacities but the slopes of the breakthrough curves were the sharpest.

The resin size may be one reason for this experimental results [4,15]. The three BSRs (PWA10, S108, and MK51) used had effective size ranges of 550–600, 425–630, and 440–540 μm, respectively [22–25]. The median values were 575, 527.5, and 490 μm, respectively. Adsorption performance is known to increase with a decrease in resin bead size. This may be due to the increase in total surface area of the resin beads with the decrease in their size. A smaller BSR has more places required to react with boron than a larger BSR does. Thus, the reaction rate of a finer BSR is faster than that of a coarser BSR. Another reason may be the decrease in diffusion resistance in small resin beads [27,30–32]. As the bead size decreases, the thickness of external film around the particle decreases, and also the total length of the path inside the pores decreases. That is, smaller resins have a shorter diffusion path, thus allowing the adsorbate ions to penetrate the adsorbent resin more quickly, resulting in a higher adsorption rate. Finally, intraparticle diffusion is the rate-limiting step and smaller beads will yield a shorter mass transfer zone (MTZ) length. Here, the MTZ, which is the length of the adsorption zone in the column, indicates efficiency in the use of adsorbents in the column.

3.2. Effects of flow rate on breakthrough curves

For a continuous flow fixed-bed column, contact time between adsorbent and adsorbate is an important factor [5,20,26,28,33–38]. One of the control parameters for adjusting the contact time is the flow rate. To assess the effect of flow rate on boron adsorption, flow rates were applied at 3, 5, and 7 L/h, with a constant bed depth of 80 cm (freeboard of 80 cm) and an influent boron concentration of 2.5 mg/L. Fig. 3

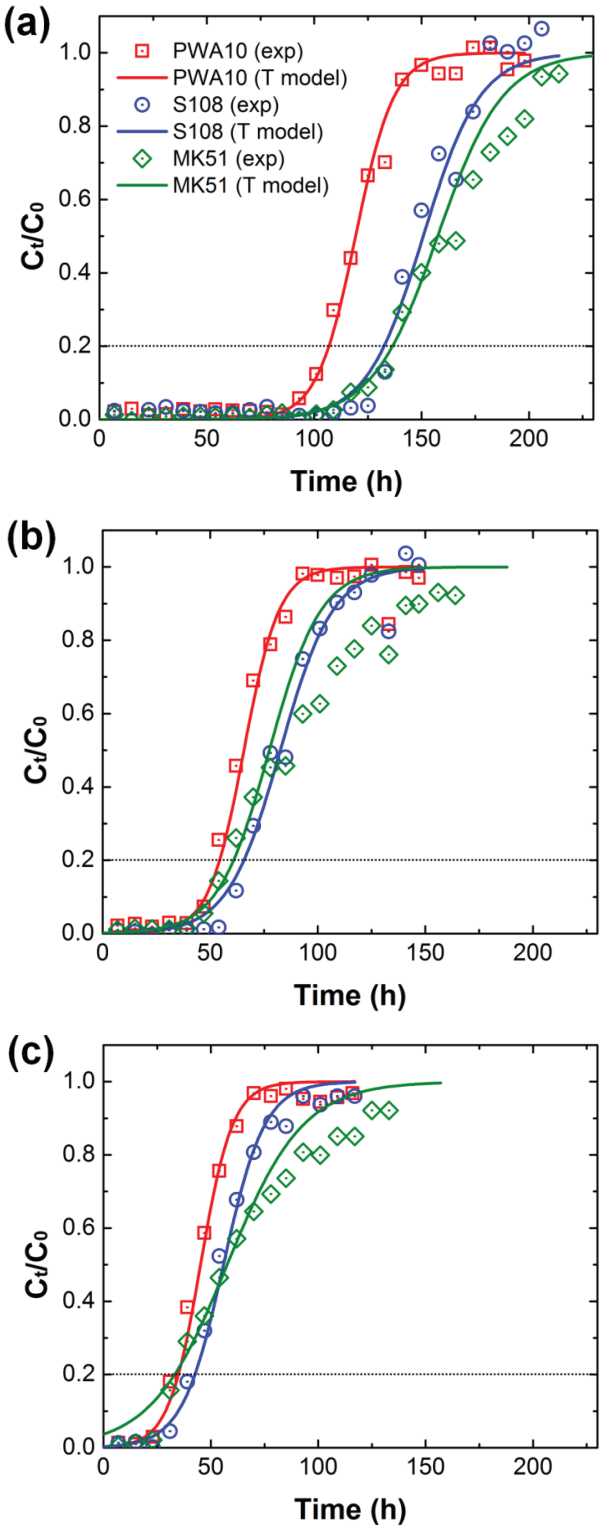

Fig. 2. Experimental and modelled boron breakthrough curves of three kinds of boron specific resins (PWA10, S108, and MK51) for different flow rates. (a) 3 L/h, (b) 5 L/h, and (c) 7 L/h. For each graph, symbols represent experimental data points and curved lines represent model results. The horizontal dotted line represents breakpoint concentration (number of columns (N_C) = 9, H = 80 cm, C_0 = 2.5 mg/L, and downflow operation).

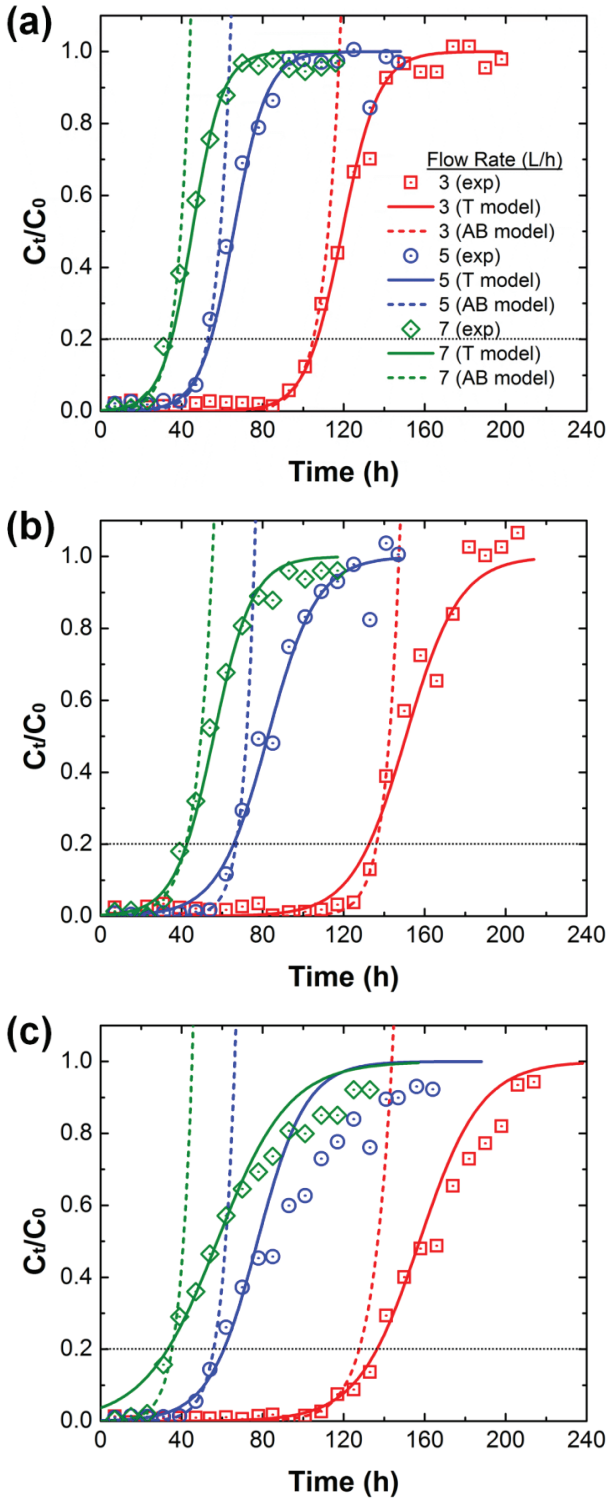

Fig. 3. Experimental and modelled boron breakthrough curves of different flow rates (3, 5, and 7 L/h) for three kinds of boron specific resins. (a) PWA10, (b) S108, and (c) MK51. For each graph, symbols represent experimental data points and solid and dotted curved lines represent Thomas and Adams–Bohart model results, respectively. The horizontal dotted line represents breakpoint concentration (N_C = 9, H = 80 cm, C_0 = 2.5 mg/L, and downflow direction).

presents the breakthrough curves at various flow rates for the three BSRs tested. Basically, at a low flow rate, adsorbate ions have enough time to diffuse into the pores of the resin beads and therefore more available functional group sites can capture ions around or inside the adsorbent bead [6,28,33]. Also, a rise in linear flow velocity increases the phenomenon of dispersion (transverse and longitudinal) in beds [39]. The dispersion coefficient in the longitudinal direction is superior to the dispersion coefficient in the radial direction for large Reynolds numbers.

The adsorption data obtained from the column studies at different flow rates were analysed using the Thomas, Yoon–Nelson, and Adams–Bohart models. For Yoon–Nelson model, model parameters were only presented in Table 3 because its curve is similar to Thomas curve. Because the Thomas and Yoon–Nelson models did not fit the experimental data well in the initial region, the Adams–Bohart adsorption model was applied to the experimental data to describe the initial region of the breakthrough curve [26,29]. In our results, the Adams–Bohart model was valid for C_t/C_0 < ~0.2. Large discrepancies between the experimental and predicted curves appeared above that value. The results shown in Fig. 3 demonstrate that there was good agreement between the experimental points and predicted normalised concentration for PWA10 resin, rather than the S108 and MK51 resins. In particular, the MTZ length of PWA10 was the shortest among the three resins. In other words, the shorter MTZ signifies the sharper slope of the curve. When the shape of the breakthrough curve is as sharp as possible, the most efficient adsorption performance is known to be obtained.

Notably, we observed that the breakthrough time was generally faster with higher flow rates, and higher flow rates resulted in shorter column exhaustion time. Generally, the practical capacity depends on flow rate and drops rapidly as flow rate increases due to mass transfer limitations. At high flow rate, the residence time of the adsorbate in the column was not long enough for adsorption equilibrium and it left the column before equilibrium occurred. The kinetic parameters of the *T*, YN, and AB models were determined from the linearised mathematical equations in Table 2. The calculated rate constants, k_{YN}, k_T, and k_{AB}, tended to increase as the flow rate increased, whereas q_e became smaller (Table 3). The breakthrough curves obtained were sharper with increasing flow rates due to the increasing rate constant.

The contact time between the adsorbent and adsorbate is called the empty bed contact time (EBCT) [28,29,33,35,37,40]. Table 3 lists the values of EBCT for each column. The EBCT, including the bed volume and flow rate, can be expressed as:

$$\text{EBCT} = \frac{V}{Q} = \frac{H \cdot A}{Q} = \frac{\pi d^2 H}{4Q}$$

Table 3
Detailed experimental conditions for investigating the effect of the different flow rates and various resin types in nine columns and the model parameters obtained from linearised forms for three models used

Column no.	1	2	3	4	5	6	7	8	9
Resin type	PWA10	S108	MK51	PWA10	S108	MK51	PWA10	S108	MK51
Bed volume (L)	0.251	0.251	0.251	0.251	0.251	0.251	0.251	0.251	0.251
Bed mass (g)	175.7	175.7	178.21	175.7	175.7	178.21	175.7	175.7	178.21
Bed depth (m)	0.8	0.8	0.8	0.8	0.8	0.8	0.8	0.8	0.8
Influent concentration (mg/L)	2.5	2.5	2.5	2.5	2.5	2.5	2.5	2.5	2.5
Flow direction	Down	Down	Down	Down	Down	Down	Down	Down	Down
Flow rate (L/h)	3	3	3	5	5	5	7	7	7
Linear flow velocity (m/h)	9.55	9.55	9.55	15.92	15.92	15.92	22.29	22.29	22.29
Specific flow rate (BV/h)	11.95	11.95	11.95	19.92	19.92	19.92	27.89	27.89	27.89
EBCT (min)	5.02	5.02	5.02	3.01	3.01	3.01	2.15	2.15	2.15
Yoon–Nelson model									
k_{YN} (h^{-1})	0.111	0.076	0.066	0.122	0.082	0.084	0.135	0.105	0.057
τ (h)	119.8	151	157.7	65.8	82.5	77.5	45.1	55.8	57.6
q_e (mg/g)	5.161	6.507	6.701	4.747	5.953	5.512	4.564	5.643	5.745
Thomas model									
k_T (L/mg h)	0.044	0.030	0.026	0.048	0.032	0.033	0.053	0.041	0.022
q_e (mg/g)	5.161	6.498	6.691	4.739	5.96	5.512	4.574	5.653	5.745
Adams–Bohart model									
k_{AB} (L/mg h)	0.049	0.058	0.040	0.058	0.070	0.061	0.063	0.048	0.064
N_0 (mg/L)	3,553.4	4,441.3	4,334.7	3,220.9	3,833.0	3,343.0	3,107.0	3,909.5	3,196.4
N_0 (mg/g)	5.076	6.345	6.105	4.601	5.476	4.708	4.439	5.585	4.502

where V is the adsorbent bed volume, Q is the solution flow rate, H is the height of the column, A is the cross-sectional area of the column, and d is the column diameter. Accordingly, changes in the bed depth, column diameter, and flow rate affect EBCT values. The EBCTs for the flow rates of 3, 5, and 7 L/h in 80 cm bed were 5.02, 3.01, and 2.15 min, respectively. These EBCT values are important for scaling up a laboratory experiment. For example, when the column diameter increases linearly, constant EBCT values should be maintained with the appropriate values of bed depth and flow rate [26,28,29]. As expected, longer run times were achieved at larger EBCTs than smaller EBCTs.

3.3. Effects of bed depth and flow direction on breakthrough curves

Another control parameter for adjusting the contact time is bed height. For this, bed heights were varied at 80, 120, and 160 cm, with a constant flow rate of 10 L/h and influent boron concentration of 2.5 mg/L. For upflow operation, no column had any freeboard. Fig. 4 presents the breakthrough curves at different bed depths. The figure clearly shows that the breakthrough times increased, from 15.5 to 31 to 47.5 h, as did the exhaustion times, from 53 to 76 to 106 h, with increasing bed heights, from 80 to 120 to 160 cm, respectively. That is, the bed was saturated in less time for smaller bed heights. This is because the increased bed height allowed a longer contact time between the adsorbent and the adsorbate. Increased bed height led to increased amounts of adsorbent, resulting in the availability of more binding sites for adsorption. Consequently, the higher bed column resulted in a lower effluent concentration in the same service time. Normally, when the bed depth increases, the value of q_e increases whereas that of k_T decreases as shown in Table 4 [18,26,28,29,33,35,38]. However, this experimental results did not precisely correspond with this trend. In particular, the data obtained from a 160-cm bed depth were lower than those with a 120-cm bed depth. Among the three bed depths tested, the best fitting of the experimental and simulated curves was observed for the bed depth of 120 cm.

Fig. 5 shows the effects of flow rate and bed depth on the pressure drop in a high-depth column. Every hydraulic system has a certain resistance, which is dependent on the flow. Likewise, the flow resistance is dependent on the column depth. Namely, the pressure drop was a function of the flow rate and bed depth and increased with increasing flow rate and bed depth. It has been reported that linear flow velocities faster than 50 m/h may bring about excessive pressure drops across a bed [21]. Of course, linear flow velocities slower than 1 m/h may also give rise to channelling inefficiency [21]. In a conventional adsorption process with a fixed-bed column, the use of high bed depth and fine beads as adsorbents brings about a significant pressure drop [4,21,41]. According to the Kozeny–Carman equation, the pressure drop (ΔP) in a fixed bed is proportional to the height (H) of the bed and inversely proportional to the square of the particle size (D_p) [4]. Accordingly, in most of the large-scale processes, relatively large resins are used to reduce pressure drop and resin cost. The pressure drop of the fixed-bed column was closely related to energy consumption. As the

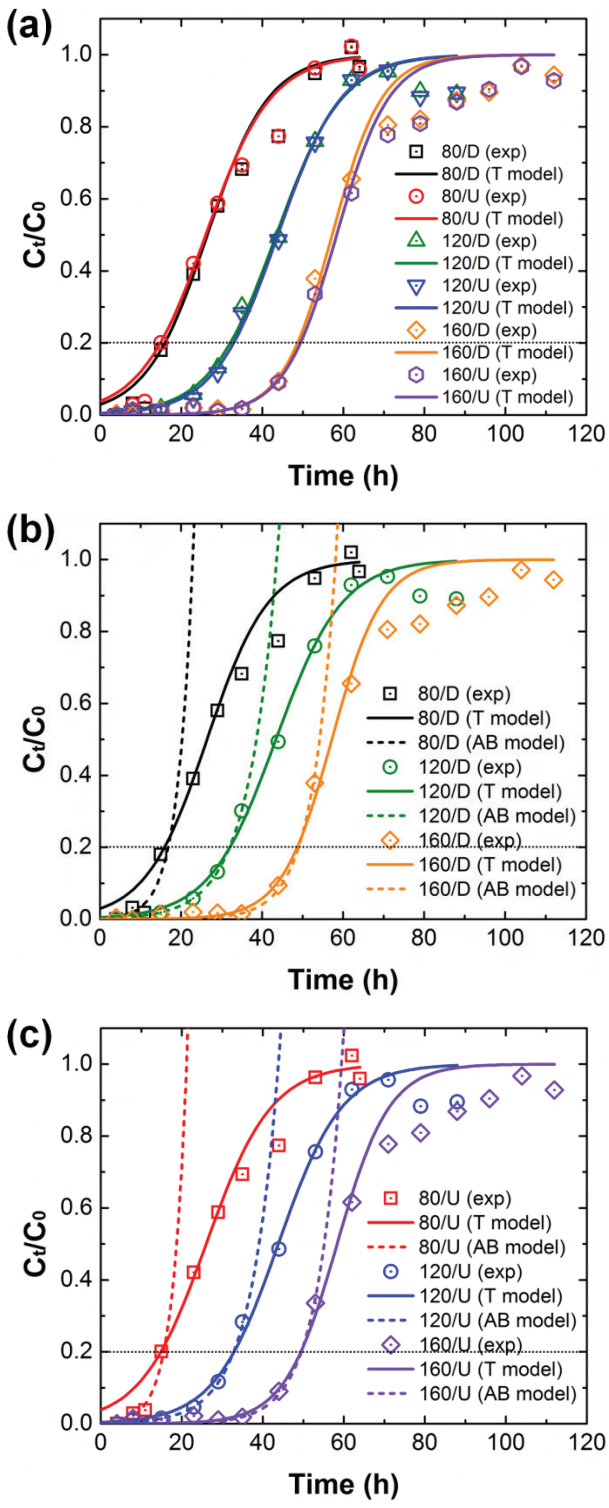

Fig. 4. Experimental and modelled boron breakthrough curves for different bed depths (80, 120, and 160 cm) and two flow directions. (a) Both upflow and downflow operations, (b) downflow alone, and (c) upflow alone. For each graph, symbols represent experimental data points and solid and dotted curved lines represent Thomas and Adams–Bohart model results, respectively. The horizontal dotted line represents breakpoint concentration (N_C = 6, BSR = PWA10, Q = 10 L/h, and C_0 = 2.5 mg/L).

Table 4
Detailed experimental conditions for investigating the effect of the different bed depths and flow direction in six columns and the model parameters obtained from linearised forms for three models used

Column no.	1	2	3	4	5	6
Resin type	PWA10	PWA10	PWA10	PWA10	PWA10	PWA10
Bed volume (L)	0.251	0.251	0.377	0.377	0.502	0.502
Bed mass (g)	175.7	175.7	263.9	263.9	351.4	351.4
Bed depth (m)	0.8	0.8	1.2	1.2	1.6	1.6
Influent concentration (mg/L)	2.5	2.5	2.5	2.5	2.5	2.5
Flow direction	Down	Up	Down	Up	Down	Up
Flow rate (L/h)	10	10	10	10	10	10
Linear flow velocity (m/h)	31.85	31.85	31.85	31.85	31.85	31.85
Specific flow rate (BV/h)	39.84	39.84	26.53	26.53	19.92	19.92
EBCT (min)	1.51	1.51	2.26	2.26	3.01	3.01
Yoon–Nelson model						
k_{YN} (h^{-1})	0.132	0.124	0.122	0.127	0.162	0.155
τ (h)	26.5	25.9	43.5	44	57.4	58.4
q_e (mg/g)	3.975	3.893	4.277	4.32	4.135	4.211
Thomas model						
k_T (L/mg h)	0.050	0.047	0.047	0.049	0.064	0.061
q_e (mg/g)	3.966	3.906	4.266	4.306	4.125	4.206
Adams–Bohart model						
k_{AB} (L/mg h)	0.101	0.108	0.053	0.056	0.070	0.064
N_0 (mg/L)	2,403.1	2,224.4	3,001.3	3,017.6	2,930.9	2,997.6
N_0 (mg/g)	3.433	3.178	4.288	4.311	4.187	4.282

depth of the bed and/or the flow rate increased, the specific energy consumption (kWh/m^3) of the pump increased as demonstrated in Fig. 5. Here, the specific energy consumption was calculated by the power consumption of pump ($W_{pump} = (P_{outlet} - P_{inlet})_{pump} \times Q_{pump} \times 1/\eta_{pump} \times 1/\eta_{motor}$) divided by the flow rate (Q_{pump}). η_{pump} and η_{motor} are the pump and motor efficiency and are assumed to be 0.7 and 0.7, respectively. The results demonstrated that the fixed-bed adsorption process consumes much less energy than a membrane process as reported by Jacob [9] and Glueckstern and Priel [10].

The differential pressure in upflow operation was lower than that in downflow operation. This may be because the packed resin bed may become a little looser in upflow operation against gravity. Upflow operation of the adsorption column can be considered to avoid liquid maldistribution and low liquid holdup [27,34,41]. That is, upflow operation is known to have higher wetting levels than downflow operation. However, in narrow columns like this experimental setup, the phenomenon of channelling will not be encountered. Consequently, the flow direction had a negligible effect on the adsorption performance in this experiment. Over 120 cm bed depths, the results in upflow mode were slightly better than those in downflow mode.

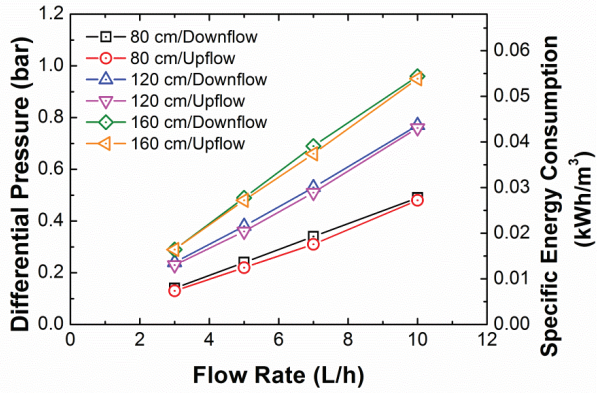

Fig. 5. Effect of the flow rate on the differential pressure for different bed depths (80, 120, and 160 cm) and two flow directions: upward and downward. (N_C = 6 and BSR = PWA10).

3.4. Effects of influent boron concentration on breakthrough curves

Fig. 6(a) compares the effects of two influent boron concentrations (C_0 = 2.5 and 5 mg/L of boron) with a constant bed depth of 80 cm and flow rates of 7 L/h. With an increase in influent boron concentration from 2.5 to 5 mg/L,

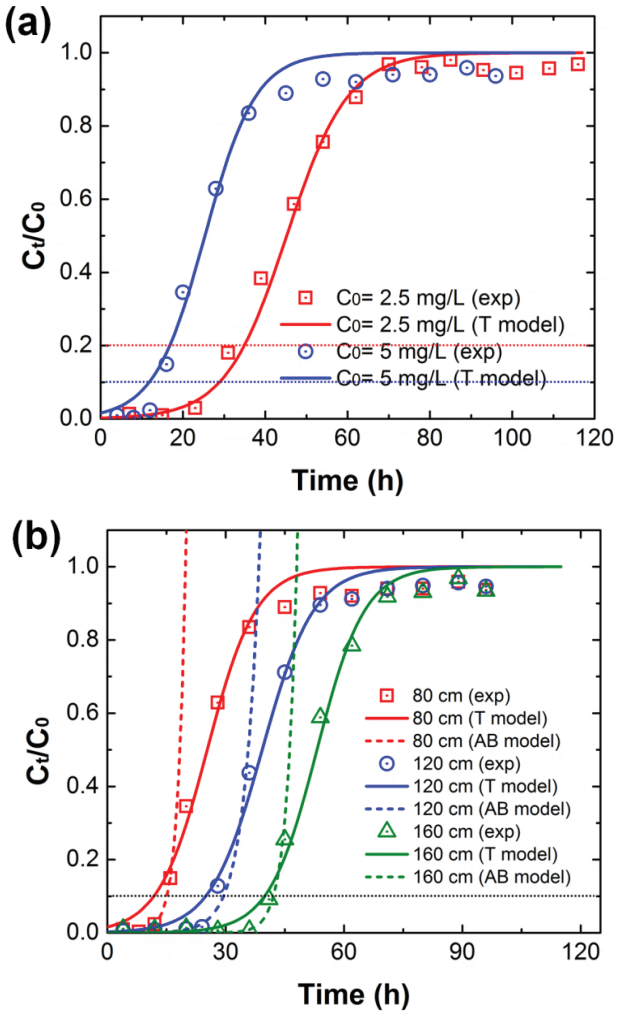

Fig. 6. (a) Experimental and modelled boron breakthrough curves of different influent boron concentrations (2.5 and 5 mg/L) (BSR = PWA10, Q = 7 L/h, and downflow direction). (b) Experimental and modelled boron breakthrough curves of different bed depths (80, 120, and 160 cm) (N_C = 3, BSR = PWA10, Q = 7 L/h, C_0 = 5 mg/L, and downflow operation). For above graph, symbols represent experimental data points and solid and dotted curved lines represent Thomas and Adams–Bohart model results, respectively. The horizontal dotted line represents breakpoint concentration.

the respective breakthrough and exhaustion times decreased. At lower influent boron concentrations, breakthrough curves were slightly dispersed and breakthrough occurred slowly. As influent concentrations increased, slightly sharper breakthrough curves were obtained. Here, the C_t/C_0 values of the breakthrough points were 0.2 and 0.1 for the influent boron concentrations of 2.5 and 5 mg/L, respectively, because the breakpoint concentration was still 0.5 mg/L. Also, as shown in Table 5, as the influent concentration increased, the value of q_e increased but the value of k_T decreased. These results indicate that the change in concentration gradient affected the breakthrough time and saturation rate. Like this, the driving force for adsorption is the concentration gradient between the boron on the adsorbent and the boron in the solution [26,33]. A higher initial influent boron concentration facilitates overall mass transfer of boron across the liquid–solid interface. As the boron concentration increases, adsorption sites are more covered [28,37], whereas a lower initial concentration of boron causes slower diffusion of boron onto the adsorbent due to the decreased mass transfer coefficient, thereby contributing to the lengthier exhaustion time of the column.

3.5. Bed depth service time analysis

Previous sections described how Thomas, Yoon–Nelson, and Adams–Bohart models, based on non-linear regression analyses, were used to fit the column adsorption data whereas the BDST model, based on linear regression analysis, was required to obtain model parameters that were useful in scale-up of the process. Generally, the BDST model is used to predict the time needed for breakthrough and exhaustion under other operating conditions [33]. A plot of time (t) vs. depth (H) yielded a linear relationship by BDST equation in Table 2 (Fig. 7(a)). Linear fits of breakthrough and exhaustion points can be expressed as t = 40 H - 16.67 and t = 66.25 H – 1.167, respectively. With an increase in the bed depth, the residence time of the fluid inside the column increases, allowing the adsorbate to adsorb more onto the adsorbent, thereby increasing the adsorption capacity with the service time.

The adsorption capacity (N_0) and rate constant (k_{BDST}) were calculated from the slope ($a = N_0 C_0^{-1} v^{-1}$) and intercept ($b = -k_{BDST}^{-1} C_0^{-1} \ln(C_0 C_t^{-1} - 1)$ of the plot, respectively. The calculated N_0 and k_{BDST} values for breakthrough points were 3,184.7 mg/L and 0.0333 L/mg h, respectively, while those for exhaustion points were 5,274.7 mg/L and 0.4753 L/mg h, respectively. k_{BDST} basically signifies the solute transfer rate from the liquid phase to the solid phase. The larger the k_{BDST} value, the higher is the performance efficiency of the bed. The higher value of k_{BDST} for the exhaustion point simply indicates more service time for the same. Accordingly, these BDST model constants can be helpful in designing the process for other flow rates and concentrations without further experimental runs [26,28] as shown in Figs. 7(b) and (c). Here, the slope constant for different flow rates was directly calculated by $a_{new} = a_{old}$ (Q_{old}/Q_{new}). For other influent concentrations, the linear equation was modified by both slope $a_{new} = a_{old}$ (C_{old}/C_{new}) and intercept $b_{new} = b_{old}$ (C_{old}/C_{new}) [$\ln(C_{new} - 1)/\ln(C_{old} - 1)$].

3.6. Sensitivity analysis

A sensitivity analysis for the Thomas model was performed under specified input conditions of a boron influent concentration of 2.5 mg/L, a bed mass of 175.7 g (i.e., height of 80 cm), a flow discharge of 3 L/h, a rate constant of 0.05 L/mg h, and an adsorption capacity of 4 mg/g. A sensitivity analysis is a technique used to determine how different values of an independent variable affect a particular dependent variable under a given set of assumptions [36]. Fig. 8 illustrates how the breakthrough curve would change with varying k_T, q_e, m, Q, or C_0. The value of k_T influenced the slope of the breakthrough curve notably. The theoretical breakthrough curves obtained were sharper with increasing

Table 5
Detailed experimental conditions for investigating the effect of the different influent boron concentrations in three columns and the model parameters obtained from linearised forms for three models used

Column no.	Column no. 7 in Table 3	1	2	3
Resin type	PWA10	PWA10	PWA10	PWA10
Bed volume (L)	0.251	0.251	0.377	0.502
Bed mass (g)	175.7	175.7	263.9	351.4
Bed depth (m)	0.8	0.8	1.2	1.6
Influent Concentration (mg/L)	2.5	5	5	5
Flow direction	Down	Down	Down	Down
Flow rate (L/h)	7	7	7	7
Linear flow velocity (m/h)	22.29	22.29	22.29	22.29
Specific flow rate (BV/h)	27.89	27.89	18.57	13.94
EBCT (min)	2.15	2.15	3.23	4.31
Yoon–Nelson model				
k_{YN} (h^{-1})	0.135	0.162	0.153	0.165
τ (h)	45.1	25.4	39.3	53.1
q_e (mg/g)	4.564	4.995	5.157	5.232
Thomas model				
k_T (L/mg h)	0.053	0.033	0.031	0.033
q_e (mg/g)	4.574	4.989	5.15	5.235
Adams–Bohart model				
k_{AB} (L/mg h)	0.063	0.098	0.052	0.079
N_0 (mg/L)	3,107.0	2,733.7	3,530.2	3,308.0
N_0 (mg/g)	4.439	3.905	5.043	4.726

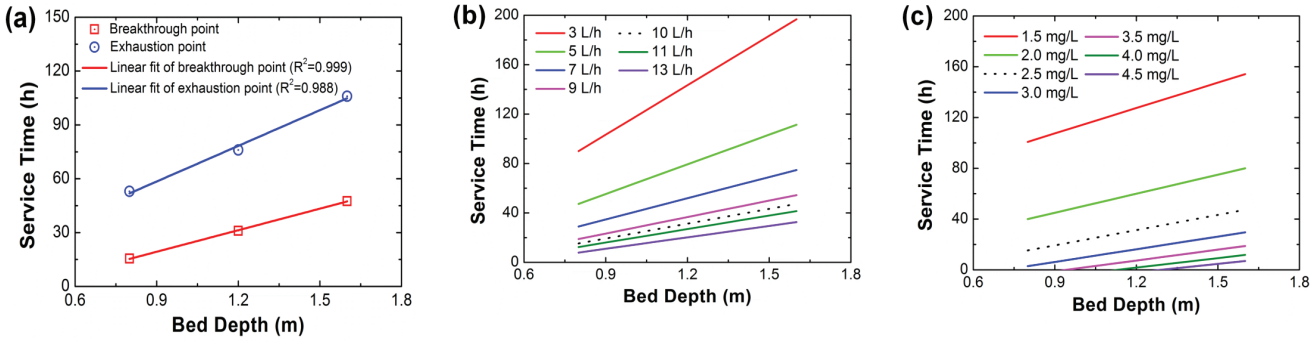

Fig. 7. (a) Analysis of breakthrough and exhaustion time by BDST model for different bed depths. For above graph, symbols represent experimental breakthrough and exhaustion points and lines represent linear fit (BSR = PWA10, Q = 10 L/h, C_0 = 2.5 mg/L, and down-flow operation). (b) Modified BDST model for different flow rates. (c) Modified BDST model for different influent concentrations. In (b) and (c), dotted line is an original BDST model of breakthrough point in (a).

rate constant due to the increasing flow rate. The 50% adsorbate breakthrough times when the value of C_t/C_0 was 0.5 were all the same. The variations in q_e, m, or Q caused a horizontal shift in breakthrough curves with the same slope, whereas their effects on the slope of the breakthrough curve were negligible. On the other hand, the change in C_0 influenced both the slope and shift of the breakthrough curve. As k_T or C_0 are decreased, the curve is elongated and flattened. Each parameter was actually dependent on each other like the relationship between flow rate and rate constant. That is, depending on the flow rate, the rate constant will be influenced. Therefore, changes in the shape and slope (length of MTZ) of the breakthrough curve can be manipulated by changing the feed flow rate and bed depth.

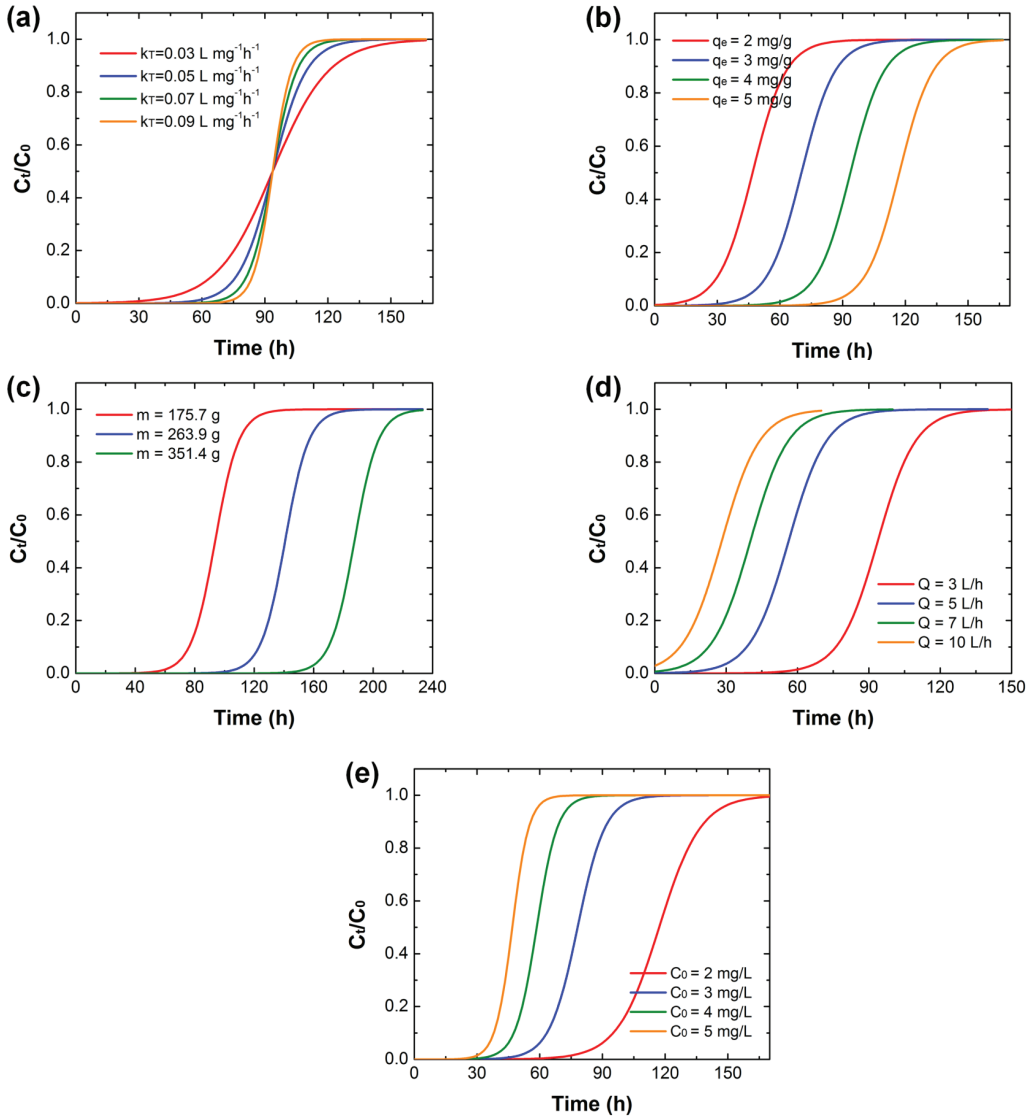

Fig. 8. Sensitivity analysis of modelled breakthrough curves for variations of following parameters. (a) Rate constant (k_T), (b) adsorption capacity (q_e), (c) bed mass (m), (d) flow rate (Q), and (e) influent boron concentration (C_0). Input parameters except variable in each graph are as follows: k_T = 0.05 L/mg h, q_e = 4 mg/g, m = 175.7 g, Q = 3 L/h, and C_0 = 2.5 mg/L.

4. Conclusions

The adsorptive removal of boron from aqueous solutions with BSRs in high-depth fixed-bed columns was investigated, experimentally and theoretically. The results regarding the relationship between adsorption performance and operating parameters can be used for the design of large-scale BSR processes. Adsorption performance was strongly dependent on the flow rate, bed depth, and influent boron concentration. Both breakthrough and exhaustion time increased with increasing EBCT (related to flow rate and bed depth), while they decreased with the increase in the influent boron concentration. The prediction results for the boron breakthrough curve using Thomas and BDST models will aid in the successful design and determination of the dynamic response of a large-scale adsorption column. Although not discussed here, it is critical to optimise the column aspect ratio to prevent maldistribution on an industrial scale. In addition, further studies on regeneration are still needed for the successful design of a large-scale BSR adsorption process. In conclusion, it seems to be sensible to use BSR adsorption instead of a second-pass RO when the TDS of the first-pass permeate meets the final specification and a low-energy process is required.

Acknowledgements

This work is supported by the Korea Agency for Infrastructure Technology Advancement (KAIA) grant funded by the Ministry of Land, Infrastructure and Transport (Grant 18IFIP-B116952-03).

References

[1] W.W. Choi, K.Y. Chen, Evaluation of boron removal by adsorption on solids, Environ. Sci. Technol., 13 (1979) 189–196.
[2] S. Sahin, A mathematical relationship for the explanation of ion exchange for boron adsorption, Desalination, 143 (2002) 35–43.
[3] K.L. Tu, L.D. Nghiem, A.R. Chivas, Boron removal by reverse osmosis membranes in seawater desalination applications, Sep. Purif. Technol., 75 (2010) 87–101.
[4] N. Hilal, G.J. Kim, C. Somerfield, Boron removal from saline water: a comprehensive review, Desalination, 273 (2011) 23–35.
[5] I.Y. Ipek, N. Kabay, M. Yuksel, Modeling of fixed bed column studies for removal of boron from geothermal water by selective chelating ion exchange resins, Desalination, 310 (2013) 151–157.
[6] E.B. Simsek, U. Beker, B.F. Senkal, Predicting the dynamics and performance of selective polymeric resins in a fixed bed system for boron removal, Desalination, 349 (2014) 39–50.
[7] J. Kluczka, T. Korolewicz, M. Zolotajkin, J. Adamek, Boron removal from water and wastewater using new polystyrene-based resin grafted with glycidol, Water Resour. Ind., 11 (2015) 46–57.
[8] M.M. Nasef, M. Nallappan, Z. Ujang, Polymer-based chelating adsorbents for the selective removal of boron from water and wastewater: a review, React. Funct. Polym., 85 (2014) 54–68.
[9] C. Jacob, Seawater desalination: boron removal by ion exchange technology, Desalination, 205 (2007) 47–52.
[10] P. Glueckstern, M. Priel, Optimization of boron removal in old and new SWRO systems, Desalination, 156 (2003) 219–228.
[11] N. Nadav, Boron removal from seawater reverse osmosis permeate utilizing selective ion exchange resin, Desalination, 124 (1999) 131–135.
[12] N. Kabay, S. Sarp, M. Yuksel, O. Arar, M. Bryjak, Removal of boron from seawater by selective ion exchange resins, React. Funct. Polym., 67 (2007) 1643–1650.
[13] N. Kabay, S. Sarp, M. Yuksel, M. Kitis, H. Koseoglu, O. Arar, M. Bryjak, R. Semiat, Removal of boron from SWRO permeate by boron selective ion exchange resins containing N-methyl glucamine group, Desalination, 223 (2008) 49–56.
[14] M.F.C. Arias, L.V. i Bru, D.P. Rico, P.V. Galvan, Comparison of ion exchange resins used in reduction of boron in desalinated water for human consumption, Desalination, 278 (2011) 244–249.
[15] N.B. Darwish, V. Kochkodan, N. Hilal, Boron removal from water with fractionized Amberlite IRA743 resin, Desalination, 370 (2015) 1–6.
[16] M. Garcia-Soto, E.M. Camacho, Boron removal from industrial wastewaters by ion exchange: an analytical control parameter, Desalination, 181 (2005) 207–216.
[17] M. Simonnot, C. Castel, M. Nicolai, C. Rosin, M. Sardin, H. Jauffret, Boron removal from drinking water with a boron selective resin: is the treatment really selective?, Water Res., 34 (2000) 109–116.
[18] A.E. Yilmaz, R. Boncukcuoglu, M.T. Yilmaz, M.M. Kocakerim, Adsorption of boron from boron-containing wastewaters by ion exchange in a continuous reactor, J. Hazard. Mater., 117 (2005) 221–226.
[19] H. Parschova, E. Mistova, Z. Matejka, L. Jelinek, N. Kabay, P. Kauppinen, Comparison of several polymeric sorbents for selective boron removal from reverse osmosis permeate, React. Funct. Polym., 67 (2007) 1622–1627.
[20] I.Y. Mohammed, K. Garba, S.D. Mandara, A.M. Saba, U.D. Sule, M. Ahmed, Comparative study of boron removal from reverse osmosis permeate using ion exchange resins, Int. J. Emerging Trends Eng. Dev., 4 (2014) 462–475.
[21] Dow Chemical Company, Lab Guide: Column Separations Using Resins and Adsorbents. Available at: http://msdssearch.dow.com/PublishedLiteratureDOWCOM/dh_015a/0901b8038015ac4e.pdf
[22] Dow Chemical Company, Product Data Sheet: Amberlite PWA10 Resin. Available at: http://msdssearch.dow.com/PublishedLiteratureDOWCOM/dh_08d1/0901b803808d1c1a.pdf?filepath=liquidseps/pdfs/noreg/177-03078.pdf&fromPage=GetDoc
[23] Dow Chemical Company, Material Safety Data Sheet: Amberlite PWA10 Ion Exchange Resin. Available at: http://www.dow.com/en-US/ShowPDF.ashx?id=090003e8806ff 183
[24] Purolite, Engineering Bulletin: Purolite S108, Available at: http://www.purolite.com/dam/jcr: 944eb48c-b0be-40c0-acd5-c9e6db9306ff/S108%20Engineering%20Bulletin.pdf
[25] Lanxess, Product Information: Lewatit MK51, Available at: http://www.lenntech.com/Data-sheets/Lewatit-MK-51-L.pdf
[26] R. Han, Y. Wang, X. Zhao, Y. Wang, F. Xie, J. Cheng, M. Tang, Adsorption of methylene blue by phoenix tree leaf powder in a fixed-bed column: experiments and prediction of breakthrough curves, Desalination, 245 (2009) 284–297.
[27] I.J. Vassilis, Ion exchange and adsorption fixed bed operations for wastewater treatment – part I: modeling fundamentals and hydraulics analysis, J. Eng. Stud. Res., 16 (2010) 29–41.
[28] P.R. Rout, R.R. Dash, P. Bhunia, Modelling and packed bed column studies on adsorptive removal of phosphate from aqueous solutions by a mixture of ground burnt patties and red soil, Adv. Environ. Res., 3 (2014) 231–251.
[29] M. Trgo, N.V. Medvidovic, J. Peric, Application of mathematical empirical models to dynamic removal of lead on natural zeolite clinoptilolite in a fixed bed column, Indian J. Chem. Technol., 18 (2011) 123–131.
[30] L. Lapidus, N.R. Amundson, Mathematics of adsorption in beds. VI. The effect of longitudinal diffusion in ion exchange and chromatographic columns, J. Phys. Chem., 56 (1952) 984–988.
[31] H. Qiu, L. Lv, B. Pan, Q. Zhang, W. Zhang, Q. Zhang, Critical review in adsorption kinetic models, J. Zhejiang Univ. Sci. A, 10 (2009) 716–724.
[32] L. Largitte, R. Pasquier, A review of the kinetics adsorption models and their application to the adsorption of lead by an activated carbon, Chem. Eng. Res. Des., 109 (2016) 495–504.
[33] E. Malkoc, Y. Nuhoglu, Removal of Ni(II) ions from aqueous solutions using waste of tea factory: adsorption on a fixed-bed column, J. Hazard. Mater., 135 (2006) 328–336.
[34] I.J. Vassilis, Ion exchange and adsorption fixed bed operations for wastewater treatment – part II: scale-up and approximate design methods, J. Eng. Stud. Res., 16 (2010) 42–50.
[35] A. Negrea, L. Lupa, M. Ciopec, P. Negrea, Experimental and modeling studies on As(III) removal from aqueous medium on fixed bed column, Chem. Bull. "Politehnica" Univ. (Timisoara), 56 (2011) 89–93.
[36] A.A. Hekmatzadeh, A. Karimi-Jashani, N. Talebbeydokhti, B. Klove, Modeling of nitrate removal for ion exchange resin in batch and fixed bed experiments, Desalination, 284 (2012) 22–31.
[37] A.B. Albadarin, C. Mangwandi, A.H. Al-Muhtaseb, G.M. Walker, S.J. Allen, N.M. Ahmad, Modelling and fixed bed column adsorption of Cr(VI) onto orthophosphoric acid-activated lignin, Chin. J. Chem. Eng., 20 (2012) 469–477.
[38] J.T. Nwabanne, P.K. Igbokwe, Adsorption performance of packed bed column for the removal of lead (ii) using oil palm fibre, Int. J. Appl. Sci. Technol., 2 (2012) 106–115.
[39] J.M.P.Q. Delgado, A critical review of dispersion in packed beds, Heat Mass Transfer, 42 (2006) 279–310.
[40] A.M. Kennedy, A.M. Reinert, D.R.U. Knappe, I. Ferrer, R.S. Summers, Full- and pilot-scale GAC adsorption of organic micropollutants, Water Res., 68 (2015) 238–248.
[41] Y. Wu, M.R. Khadilkar, M.H. Al-Dahhan, M.P. Dudukovic, Comparison of upflow and downflow two-phase flow packed-bed reactors with and without fines: experimental observations, Ind. Eng. Chem. Res., 35 (1996) 397–405.